

Surface morphology, structural and electrical properties of electrodeposited Fe₈₅Ni₁₅/ITO films

Fatima Nemla^{a,b}, Djellal Cherrad^{*,c}, M.S.Aida^b, A. Layadi^d

^a LEPCM, Department of physics, University of Batna, Algeria.

^b Thin films and interfaces laboratory, Department of physics, Mentouri University, Constantine 25000, Algeria.

^c Laboratory for Developing New Materials and their Characterizations, University of Setif, Algeria.

^d L.E.S.I.M.S., Département de Physique, Université Ferhat Abbas, Sétif 1, Sétif 19000, Algeria

Abstract

Series of Fe₈₅Ni₁₅ films have been grown on tin-doped indium oxide (ITO)-coated glass substrates by the electrodeposition technique. The samples were made using different chemical potentials and deposition times, t. The structural properties and the surface morphology have been studied by the X-ray diffraction (XRD), scanning electron microscope, equipped with high power optics thermal field Emission (SEM–TFE) and a surface profilometry. The electrical properties were inferred from Hall effect measurements. The texture, lattice parameter, grain size, surface roughness, sheet resistance and electrical resistivity have been investigated. As the deposition time t increases, a change in texture from <110> to <211> is observed. This change strongly affects grain size, surface roughness behaviors and the electrical properties. These various experimental results will be discussed and correlated.

Keywords: A. Thin films, A. NiFe alloy, C. X-ray diffraction, D. electrical properties.

PACS: 73.61.At, 81.20.-n, 75.50.Bb, 07.85.Jy, 81.10.-h

*Corresponding author. Tel.: +213 661306169;

E-mail adress: cherradphisc@yahoo.fr (Djellal Cherrad).

1. Introduction

The properties of electrodeposited Ni-Fe alloys are dramatically affected by the composition, substrate roughness, crystal size, structure and internal stress in the deposits. In turn, these parameters very much depend on the current density, agitation, and other plating variables [1]. Harty *et al.* [2] indicated that an increase in the current density decreases the amount of nickel that can be co-deposited with iron. They explain this behavior by the change in the cathode potential to less noble values as the current density is increased, the electrodeposition conditions then favoring the discharge of iron, the less noble metal. Gamburg *et al.* [3] suggested that for some alloy systems such as Ni-Fe, the convergence of the deposition potentials of the two components can be the result of the alloy binding energy, i.e., purely thermodynamic factors. A lot of attention has been focused on the study of the magnetic [4] and mechanical [5] properties of nanocrystalline NiFe alloys. NiFe alloys are known to form soft magnetic coatings. The composition of soft magnetic alloys and their properties have been reported in earlier works of Morika and Tanhaschi [6], Wolf [7,8], Wolf and Katz [9], Bozart [10], Tsu and Sallo [11], Smith *et al.* [12] and Avdeeva [10]. Such NiFe alloys deposited from chloride, sulphate, mixed or sulphamate baths have been reported to be among the most interesting because they yield films with the lowest internal stress [14].

The deposition of Ni-Fe alloy is called abnormal [15] because of the fact that the less noble element (iron) is preferentially deposited before the noblest (nickel) element, therefore, the amount of iron in the deposit will not be in the same proportion as in the electrolyte. From a sulphate bath, Dahms *et al.* [16] studied electrodeposited NiFe on a rotating electrode. They found that the increase in the deposited iron amount is directly related to a decrease in the velocity of the nickel deposition. Krause *et al.* [17] have shown that abnormal codeposition plating of NiFe alloy is due, essentially, to iron hydroxide $\text{Fe}(\text{OH})_2$ precipitation at the surface of the electrode.

In the present work, we have grown FeNi alloy thin films onto tin-doped indium oxide (ITO)-coated glass substrates by the electrodeposition technique. The samples were made at different chemical potentials, E , and deposition times, t . The objectives of the present work are to investigate (i) the structural properties (texture, lattice parameter and grain size) and the surface morphology as a function of deposition time and chemical potential, (ii) the electrical properties (sheet resistance and electrical resistivity) of these samples and (iii) the relationship between different properties (structural parameters, electrical resistivity and morphological properties) as a function of the electrodeposition time (600, 720, 840, 960, 1080 and 1200 seconds).

2. Experimental details

Series of FeNi alloy thin films were prepared by electrodeposition onto polycrystalline indium tin oxide (ITO) covered glass substrate. All the depositions were made in a three electrode cells containing Ni as a counter electrode, silver-silver chloride (Ag/AgCl) as reference and ITO coated glass as a working electrode. We have chosen the ITO substrate as cathode because of its high transparence and its properties as inert material. Before deposition, the substrates were first cleaned with acetone for 30 minutes, then with alcohol for 30 min and finally rinsed in distilled water. The thin films alloys were deposited in the parstat 2253 potentiostat/galvanostat system equipped with electrochemistry PowerSuite software. The electrolyte [0.1] was freshly prepared according to the electrolytic composition (see Table 1).

Table 1: Sulfate bath electrolyte composition and the used parameters for Fe₈₅Ni₁₅ samples.

Bath composition	0.036 M NiSO ₄ ·6H ₂ O 0.064 M (NH ₄) ₂ Fe (SO ₄).6H ₂ O 12.5g NaCl 0.5 g H ₃ BO ₃ 0.2C ₁₂ H ₂₅ NaO ₄ S 0.5 Saccharin pH 2.7
Operating parameters	Temperature (°C) 20-25
Cathode	ITO
Anode	Ni

Boric acid (adjusted to 2.7 using diluted H₂SO₄) was added to the bath in order to control the pH of the solution and also to improve the quality of the deposit. In addition, Saccharin has been used as an organic additive to reduce the internal stress of deposits and to refine the grain structure [18]. FeNi thin films were deposited at a cathode potential of -1.45 (vs. Ag/AgCl) for different deposition times. After careful test, we have deduced that this potential was the best one to reach higher electrochemical deposition efficiency. Thus, all samples were obtained at this potential. Electrodeposition was performed at room temperature, without stirring.

The films thicknesses (e) and the root mean square (*rms*) surface roughness were measured by means of a Veeco Dektak 150 surface profilometer. The structural characterization of the sample was determined by X-ray diffraction (XRD) analysis, using a Philips X'Pert diffractometer with CuK α ($\lambda=1.54$ Å) radiation. Surface images and alloy composition were obtained by means of a Scanning Electron Microscope, high power optics Thermal Field Emission (SEM –TFE) JSM 7001F/ JSM 7001FA. The sheet resistance and the electrical resistivity were inferred from a Hall effect measurements set-up (using the ECOPIA HMS-3000 system from Bridge Technology).

3. Results and discussion

Two series of samples were prepared. The first one consists of samples made at the same deposition time (600 seconds) and with four different potentials: -1.45, -1.46, -1.47 and -1.48 V.

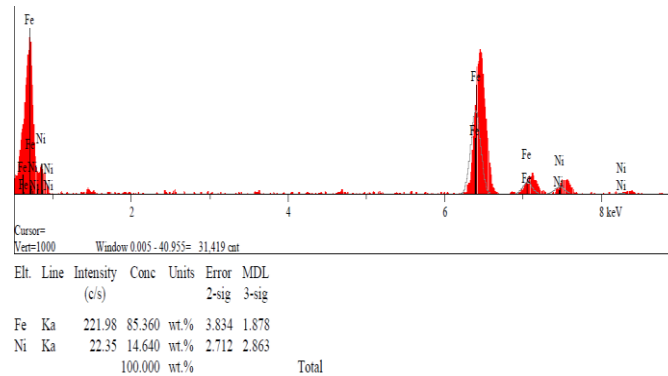


Figure.1

Fig. 1 : Example of EDX spectrum (sample elaborated at a deposition time equal to 1200 s).

The second series consists of six samples made at a fixed chemical potential (-1.45V) and for different deposition times ranging from 600 to 1200 seconds. The chemical analysis shows that the Fe content in the alloy amounts to $85 \pm 1\%$ for most samples, see Fig. 1 for an example of EDX spectrum. However two samples are found to have lower (82%) and higher (92%) Fe content. The thickness is found to monotonously increase from 520 to 1400 nm as the deposition time t increases from 600 to 1200 seconds.

In the following the structural properties (texture, lattice parameter and grain size), the surface morphology, the surface roughness, the sheet resistance and the electrical resistivity will be discussed.

3.1. Structural properties

First, we discuss The X-ray diffraction results pertaining to a set of samples prepared at room temperature with different electrochemical potential and a fixed deposition time. In Fig. 2a, we show the XRD patterns of $Fe_{85}Ni_{15}$ thin films deposited at different potentials: -1.45, -1.46, -1.47 and -1.48 V, with a deposition time set at 600 seconds. Besides the peaks marked with star (*) which are assigned to the ITO substrate, four other peaks appear at 2θ values equal to 41.65° , 44.28° , 47.6° and 51.50° ; these peaks are attributed, respectively, to the $\langle 110 \rangle$, $\langle 200 \rangle$, $\langle 220 \rangle$ and $\langle 211 \rangle$ peaks of the body centered crystal (bcc) structure. Thus, all these samples have a polycrystalline bcc structure. This result about the bcc structure is expected for our films with high Fe content, i.e the crystalline structure of the alloy follows that of the dominating chemical element in the compound. In this context, I.Tabakovic et al [19] have reported that X-ray investigation of electrodeposited NiFe films at room

temperature reveal the existence of fcc or γ phase in the range of 10-58 wt.% Fe, mixed fcc/bcc phase in the range of 59-63 wt.%, and purely bcc or α phase in the range of 64-90 wt.% Fe. In similar fashion, B. Liu *et al* [20] have noted that the permalloy $\text{Ni}_{80}\text{Fe}_{20}$ phase is that of Nickel.

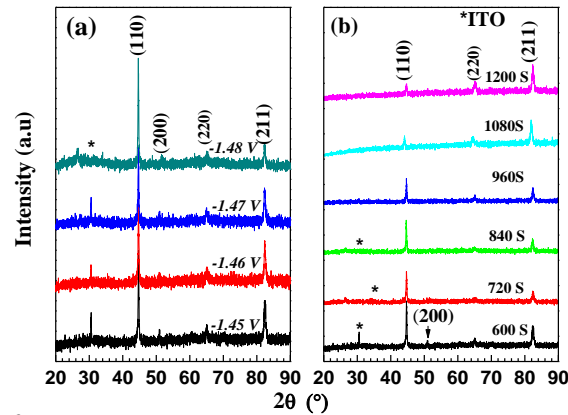


Figure.2

Fig. 2: XRD patterns for samples prepared (a) at different potentials (as indicated) and a fixed deposition time (600 seconds) and (b) at different deposition times with fixed chemical potential (-1.45V). [* denotes ITO diffraction peaks].

Furthermore, from the intensity ratios, we inferred that the texture is along the $\langle 110 \rangle$. We note here that our result about the overall texture is consistent with those of Chang Su-wei *et al* [21] who found that the $\langle 110 \rangle$ orientation is the preferred and dominant one for the structure. The same authors also suggested, in an other report, that the orientation must follow the (111) plane for a fcc structure [19,21].

We turn now to the effect of the deposition time. In Fig. 2b, we show X-ray patterns for samples prepared at different deposition times as indicated in the figure and with the same chemical potential (-1.45 V). We noted that the intensity of the (110) peaks decreases as the time deposition increases from 720 to 1200 seconds, while the (211) peak intensity increases; by computing the intensity ratios of the peaks, we may infer that there is a change of texture from $\langle 110 \rangle$ at low deposition time to $\langle 211 \rangle$ for high deposition time. The transition from $\langle 110 \rangle$ to $\langle 211 \rangle$ occurs at a critical deposition time t_c about 960 s corresponding to a critical thickness equal to $e_c = 720$ nm. This change in the texture from $\langle 110 \rangle$ to $\langle 211 \rangle$ has been observed by B. Ghebouli *et al.* [22] in pure Fe thin films evaporated onto glass substrate but in different thickness range (6 to 110 nm).

As for the lattice parameter, we have measured values between 2.8533 and 2.8692 nm. Thus the deposition time (or equivalently the thickness) did not greatly affect the lattice parameter, the difference amounts to less than 1% (about 0.55 %). Even the two samples whose Fe contents are slightly different from 85% have lattice constants within this small interval. Note that the lattice parameter for pure iron is 0.286629 ± 0.0005 nm. In ferromagnetic particulates and for a composition

close to the one of the present work, R. Hamzaoui et al [23] measured lattice parameter values between 0.286599 (± 0.00005) and 0.287049 (± 0.00005) for Fe₉₀Ni₁₀ alloy and from 0.286589 (± 0.00005) to 0.287069 (± 0.00005) nm for Fe₈₀Ni₂₀ alloy; the values we found here fall within these reported values. Also, Xiaobai Chen et al [24] have discussed the structural phase transformation and found for sputtered FeNi thick films that the lattice parameter is 0.28442 nm for the as-deposited Fe₇₉Ni₂₁, while for annealed Fe₆₇Ni₃₃ film at 753K, it amounts to 0.35866 nm; the authors noted also that these lattice parameters are smaller than the bulk one.

The grain sizes have been derived from X-ray diffraction following the Scherrer method. The grain size D for a grain with a particular orientation is given by:

$$D = \frac{0.9\lambda}{(\Delta\theta) \cos \theta} \quad (1)$$

where λ is the X-ray wavelength, θ the diffraction angle and $\Delta\theta$ is the width at half height of the peak corresponding to a particular orientation.

The grain size values D are plotted against the deposition time t in Fig. 3. We note that D decreases with increasing t up to t = 960 s, then D increases with t.

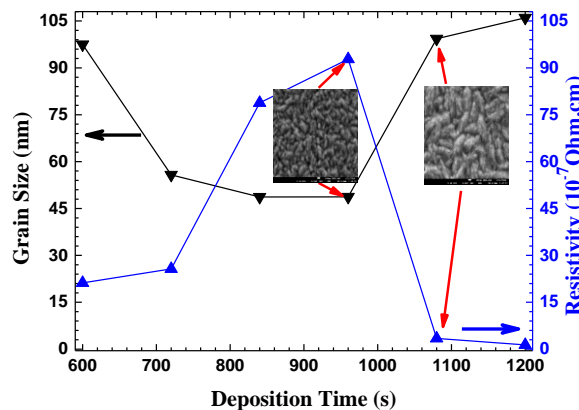


Figure.3
Fig. 3 : Grain size and electrical Resistivity versus deposition time.

Note that between 720 s and 960 s, the grain size is practically constant within the measurement uncertainties. It is interesting to note that the change in the D behavior seems to follow the change in the film texture, i.e. D decreases with t in the region where the texture is <110> and once the texture changes to <211>, D starts to increase with t. It is believed that the <211> crystalline texture is characterized by an easy diffusion at grain boundaries, leading thus to an increase in the grain size.

3.2. Surface morphology

Fig. 4 displays the surface morphology of the Fe₈₅Ni₁₅ films prepared at different deposition times. We can note by comparing SEM images ((a) to (f)), that the surface morphology is strongly influenced by the deposition time (or film thickness). The surfaces are characterized by grains with different sizes and shapes. The results inferred from SEM images agree with those derived from X-ray diffraction; see also the inset of Fig. 3 where SEM images are displayed for two samples, one can see a clear increase in the grain size with increasing deposition time beyond the critical time.

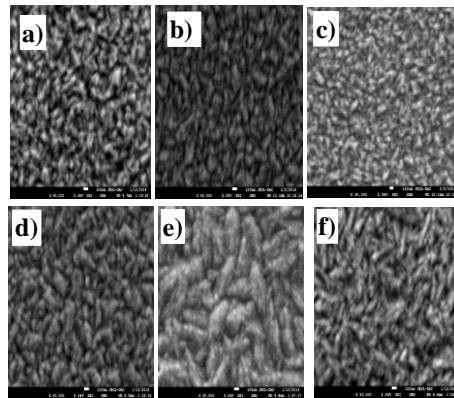


Figure.4

Fig. 4 : SEM images of Fe₈₅Ni₁₅ ($\times 40\ 000$) films prepared at different deposition times: a) t = 600s, b) t = 720s, c) t = 840s, d) t = 960s, e) t = 1080s and f) t = 1200s.

3.3. Surface roughness

In Fig. 5, we show typical and qualitative surface roughness profiles for the Fe₈₅Ni₁₅ alloy elaborated at various electrochemical potential depositions (Fig.5a) and at different deposition times (Fig.5b). For a more accurate analysis of the surface, the scan was carrying out Vertically/Horizontally in a large bidimensional range of about 0.6 μ m/5mm.

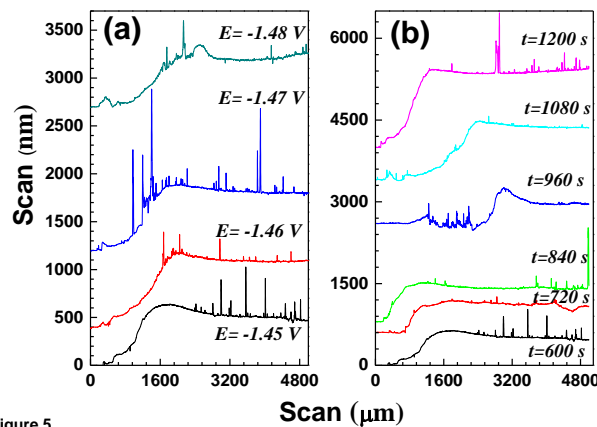


Figure.5

Fig. 5: Surface profiles for Fe₈₅Ni₁₅ samples prepared: (a) at different potential and (b) at different deposition times.

Generally, both high and deep irregularities are considerably small and reflect the efficiency of the deposition technique. However, one can note that the sample made at - 1.47 V contains more high and deep irregularities compared to other samples (see the left hand side of Fig.5a). For the effect of deposition time (see Fig. 5b), one sees that the sample made at 1080 seconds present less irregularities than the others do. From these profiles, we have measured the surface roughness; the rms values are plotted against the deposition time in Fig. 6. Here too, we clearly see the effect of texture on the surface roughness values. We note that besides the first point at 600s which happens to be the one with the highest Fe content (92%), for all other samples, the rms values increase with increasing deposition time t in the region where the texture is $\langle 110 \rangle$ ($t < t_c$); beyond the critical time t_c when the texture becomes $\langle 211 \rangle$, the rms values start to monotonously decrease with t .

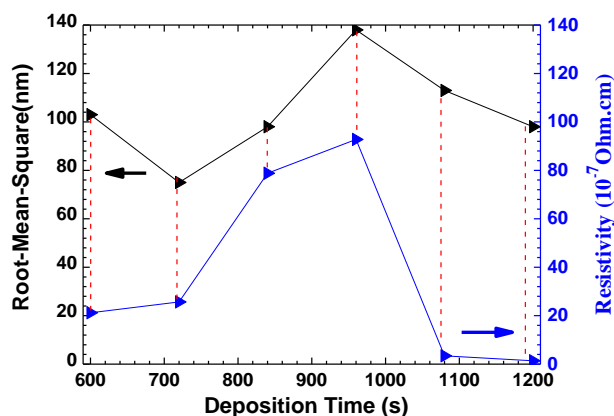


Figure.6

Fig. 6 : The root-mean-square (rms) surface roughness and electrical resistivity versus deposition time.

It should be noted here that for the series made at fixed deposition time and different potentials, the texture (<110>) did not change with the variation of the potential. Also, we did not observe a clear, monotonous variation of the other structural parameters, there is however a general trend : when the potential increases (in absolute value) from -1.45V to -1.48V, the grain size increases from 97.5 to 114.5nm, the thickness slightly decreases from 520 to 506nm and the surface roughness (rms) decreases from 103 to 88nm.

3.4. Electrical properties

From the Hall effect measurement set-up, the sheet resistance R of the Fe₈₅Ni₁₅ thin films is given by:

$$R = \frac{R_{sq} \cdot R_{sq1}}{R_{sq1} - R_{sq}} \quad (2)$$

where R_{sq} and R_{sq1} are respectively the total and the ITO film (covering the dielectric glass substrate) sheet resistances. The sheet resistance called also the sheet resistance is sometimes noted R_{\square} and is measured in Ohms/square (Ω/\square). Note that ITO has a sheet resistance equal to 10 Ω (measured in area of $1 \times 2 \text{ cm}^2$ exposed to the electrolyte). The sheet resistance R values have been measured for all samples. We note that there is first an increase of the sheet resistance from 0.041 Ω at $t = 600$ seconds (corresponding to a thickness $e = 520 \text{ nm}$) up to 0.131 Ω at $t = 960$ seconds ($e = 720 \text{ nm}$), then a decrease down to 0.001 Ω at $t = 1200$ seconds ($e = 1400 \text{ nm}$). Once again we note a correlation between the texture and the sheet resistance R; R increases with t when the texture is <110> and begins to decrease with t after the transition to the <211> texture.

The electrical resistivity ρ is related to the sheet resistance R by

$$\rho = Re \quad (3)$$

where e is the film thickness. The variation of electrical resistivity with deposition time is shown in Fig.3 along with the grain size and also in Fig. 6 with the surface roughness (rms) values; this will enable us to easily correlate between the behavior of ρ and the variations of the D and the rms values. We note that the electrical resistivity increases with t up to the critical time $t_c = 960 \text{ s}$, i.e. in the part where the texture is <110>. When the texture changes to <221>, ρ sharply decreases with t. For the comparison with the rms values (see Fig. 6), we note that, except for first point at 600s as pointed out before (the sample with a high Fe content), for all other samples, the rms values and ρ have the same behavior; both of them increase for $t < t_c$ (<110> texture) and decreases with t for $t > t_c$ (<211> texture).

These different variations of ρ with D and the rms values may give insight into the different factors contributing to the electrical resistivity values. Several phenomena can contribute to the thin

film electrical resistivity such as the diffusion by the surface, diffusion by the grain boundaries, impurities, defects and magnetic disorder and the high preferred orientation. First, one notes that the resistivity and the rms values have the same variation with the deposition time t , regardless of the texture. High rms values led to a high resistivity. Second, for the effect of the grain size, one can see from Fig.3 that for $t > t_c$, the sharp increase in the grain size led to a sharp decrease in the electrical resistivity. This indicates that the diffusion at the grain boundaries may be the major factor in the electrical resistivity, i.e. higher grain size means a low number of grain boundaries, thus less diffusion at the grain boundaries and consequently a lower resistivity. When $t < t_c$, the effect of grain boundaries is not so obvious, we observe that over a deposition time range ($720 < t < 1080$ s), the grain size remains practically constant and yet the electrical resistivity increased by a quite large amount. In this region, the main contribution to the resistivity might be the surface roughness and the texture.

Finally, we noted that, for a fixed deposition time, increasing (in absolute value) the chemical potential from -1.45 to -1.48V led to a decrease of both the sheet resistance from 0.0408 to 0.0088 Ω and the electrical resistivity from 2.1 to 0.4×10^{-6} Ω cm. We believe that the decrease in R and ρ is due to the increase of the grain size and a decrease of the surface roughness as mentioned earlier.

Conclusion

We investigated the structural and electrical properties of Fe₈₅Ni₁₅ alloy thin films grown onto ITO-coated glass substrates by electrodeposition. As the deposition time increases, we observed a change in the texture from $\langle 110 \rangle$ to $\langle 211 \rangle$. This transition occurs at a critical deposition time $t_c = 960$ seconds (corresponding to a critical thickness $e_c = 720$ nm). In the region where the texture is $\langle 110 \rangle$ ($t < t_c$), the grain size D decreases with t , while the surface roughness rms, the sheet resistance R and the electrical resistivity ρ increases; once the texture changes to $\langle 211 \rangle$ ($t > t_c$), D starts to increase with t , the rms, R and ρ decreases. We expect that these changes in the structural parameters and surface morphology may induce interesting behavior in the magnetic properties of this ferromagnetic Fe₈₅Ni₁₅ alloy, this can be a subject of a future work. Furthermore, the electrical resistivity is found to be proportional to the surface roughness. We believe that texture, surface roughness and the diffusion at the grain boundaries are the main origin of the electrical resistivity. The latter one is clearly predominant for $t > t_c$, when the texture is $\langle 211 \rangle$. For the series made at fixed deposition time and different potentials, the texture ($\langle 110 \rangle$) did not change with the variation of the potential; increasing (in absolute value) the chemical potential from -1.45 to -1.48V led to an increase in the grain size and a decrease in the surface roughness (rms), in the sheet resistance and in the electrical resistivity. We believe that the decrease in R and ρ is a consequence of the increase of the grain size and a decrease of the surface roughness.

References:

- [1] S. S. Djokic and M. D. Maksimovic, Modern Aspects of Electrochemistry, Number 22, edited by John O'M. Bockris et al. Plenum Press, New York 1992. pp 418.
- [2] F. HARTY, J. A. McGEOUGH and R. M. TULLOCH. Surf. Technology **12** (1981) 39-55.
- [3] Y. D. Gamburg, G. Zangari, Theory and Practice of Metal Electrodeposition, Book chapter, Springer New York 2011, pp 205-232
- [4] Aravinda CL, Mayanna SM. Trans IMF. **77** (1999) 87.
- [5] Li HQ, F. Ebrahimi Mater. Sci. Engineer. A **347** (2003) 93.
- [6] S. Morioka and M. Tanahaschi, J. Jpn. Inst. Met. **25** (10) (1961) 683.
- [7] J. W. Wolf, J. Am. Electroplaters'Soc. **121** (1957) 1.
- [8] J. W. Wolf, Proc. Am. Electroplaters'Soc. **43** (1956) 215.
- [9] J. W. Wolf and H. W. Katz, Proc. *Electronic Component Conf.*, Philadelphia, PA, 1959, pp. 15-20.
- [10] R.M. Bozart, Phys. Rev. **26** (1925) 390.
- [11] J. Tsu and J. Sallo, U.S. Patent **3** (031) (1962) 386.
- [12] R. S. Smith, L. E. Godicki and J. C. Lloyd, J. Electrochem. Soc. **108** (8) (1961) 779.
- [13] T. B. Avadeeva, U.S.S.R. Patent. **155** (1964) 072.
- [14] V.I. Lainer, Vestn. Mashinostr. **1** (1964) 32.
- [15] A. Brenner, "*Electrodeposition of Alloys, Principle and Practice*", Volume 1, Academic Press, New York and London, (1963).

- [16] H. Dahms, J. M. Croll, J. Electrochem. Soc. **112** (1965) 771.
- [17] T. Krause, L. Arulnayagam, M. Pritzker, J. Electrochem. Soc. **144** (1997) 960.
- [18] B. Qi, X. Ni, D. Li, H. Zheng, Chem. Lett. **37** (2008) 336.
- [19] Ibro Tabakovic, Venkateswara inturi, Jeremy Thurn, Mark Kief, Electrochem. Acta **55** (2010) 6749.
- [20] B. Liu, R. Huang, J. Wang, H.M. Widatallah, H. Lu, J. Zhang, J.Liu, J. Appl. Phys. **85** (2) (1999) 1010.
- [21] Chang-wei Su, Feng-jiao He, Hui Ju, Yu-bin Zhang, Er-Li Wang, Electrochimica Acta. **54** (2009) 6257.
- [22] B. Ghebouli, S.M.Chérif, A. Layadi, B. Helifa, M. Boudissa, J. Magnetism. Magnet. Mater. **312** (2007) 194.
- [23] R. Hamzaoui , O. Elkedim , N. Fenineche , E. Gaffet , J. Craven , Mat. Sci. Engineer. A **360** (2003) 299-305
- [24] Xiaobai Chen, Hong Qiu, PingWu , Fengping Wang, LiqingPan , Yue Tian, Phys. B. **362** (2005) 255.